Fabrication and characterisation of electro-brush plated nickel-graphene oxide nano-composite coatings

Qi, Shaojun; Li, Xiaoying; Zhang, Zhenxue; Dong, Hanshan

DOI:
10.1016/j.tsf.2017.06.064

Document Version
Peer reviewed version

Citation for published version (Harvard):
Qi, S, Li, X, Zhang, Z & Dong, H 2017, 'Fabrication and characterisation of electro-brush plated nickel-graphene oxide nano-composite coatings', *Thin Solid Films*, vol. 644, pp. 106-114. https://doi.org/10.1016/j.tsf.2017.06.064

Fabrication and characterisation of electro-brush plated nickel-graphene oxide nano-composite coatings

Shaojun Qi, Xiaoying Li, Zhenxue Zhang, Hanshan Dong

PII: S0040-6090(17)30691-0
DOI: doi:10.1016/j.tsf.2017.06.064
Reference: TSF 36224

To appear in: *Thin Solid Films*

Received date: 24 March 2017
Revised date: 7 June 2017
Accepted date: 9 June 2017

Please cite this article as: Shaojun Qi, Xiaoying Li, Zhenxue Zhang, Hanshan Dong, Fabrication and characterisation of electro-brush plated nickel-graphene oxide nano-composite coatings, *Thin Solid Films* (2017), doi:10.1016/j.tsf.2017.06.064

Fabrication and characterisation of electro-brush plated nickel-graphene oxide nano-composite coatings

Shaojun Qi, Xiaoying Li*, Zhenxue Zhang, Hanshan Dong

School of Metallurgy and Materials, University of Birmingham, Birmingham B15 2TT, UK

Abstract

The extraordinary mechanical and anti-corrosion properties of graphene call for facile fabrication of graphene-based coatings with high uniformity and in large area. This research was aimed at exploring the use of an electro-brush plating technique for the production of graphene-metal nano-composite coatings. Graphene oxide (GO) was introduced into the nickel plating solution at varied concentrations and composite coatings were fabricated on stainless steel surfaces by brush plating under the same conditions. The morphology and microstructure of the obtained Ni-GO composite coatings were fully characterised and compared with neat Ni coating. The results confirm that GO sheets have been incorporated into the nickel matrix homogeneously, leading to a considerably reduced average crystallite size. Nanoindentation measurements demonstrated that GO can not only improve the hardness and reduce the plasticity of the composite matrix, but also enhance the thermal stability of the composite coating effectively. It has also been revealed by polarisation and electrochemical impedance spectroscopy (EIS) analysis that GO can increase the corrosion resistance of the composite coating owing to its barrier effect. However, it was also noticed that excessive GO content resulted in a degradation of both mechanical and corrosion properties, likely due to a more defective microstructure.

Key words: Graphene oxide; Nano-composite coating; Nanoindentation; Thermal stability; Electrochemical impedance

* Corresponding author.
E-mail address: x.li.1@bham.ac.uk (X. Li)

1. Introduction

Graphene is a young yet very attractive carbon material owing to its extraordinary properties. Its unusual electronic properties have made it at the centre of post-silicon era research [1]. Due to an astonishing intrinsic strength of 130 GPa and a Young's modulus of 1.0 TPa [2], graphene is often cited as the strongest material ever. It has also been demonstrated that graphene is theoretically impermeable to all molecules and ions, suggesting it an ideal corrosion barrier [3]. However, unlike the well-documented research on the electronics and optoelectronic of graphene, the utilisation of its mechanical and anti-corrosion properties usually requires graphenes in larger area or as part of a surface coating formula. Notwithstanding the fact that the potential of graphene for mechanical strengthening, tribology and anti-corrosion has been demonstrated by some nano/micro studies [4-6], its macro scale application as strengthening and protective coating materials has yet to be fully explored. This is mainly due to the extremely low yield of pristine graphene by mechanical exfoliation, and the still high cost of CVD-grown graphene and the difficulties in transferring the graphene onto foreign engineering surfaces with necessary bonding.

One possible solution is to use graphene oxide (GO) for graphene-based composite coatings. GO is advantageous over other graphene derivatives in terms of its low cost, mass production and high chemical activities [7]. GO has been used in the production of various types of composite materials, including polymer [8], inorganic [9] and metallic [10] matrixes. For example, Min et al. [11] found that the incorporation of GO not only improved the mechanical and tribological properties of the polyimide matrix but also enhanced the thermal stability of the composite. The effect of GO was believed to stem from the oxygen functional groups in GO which can help form a strong interface with the polymeric matrix. In another report, a GO-hydroxyapatite (HA) composite coating was prepared on commercially pure (CP) Ti substrate by vacuum cold spraying. The GO reinforced HA coating was superior to pure HA as evidenced by better interface bonding, a 4-time increase in fracture toughness and

remarkably improved biocompatibility [9].

Metal matrix nano-composite coatings have also received much research interest due to their enhanced mechanical, tribological and corrosion performance compared with the pure metallic coating [10, 12]. They are attractive in both academic and industrial viewpoints with regards to their high compatibility to engineering surfaces, which are mostly metallic, such as steel. Nickel is widely employed as the matrix material for metallic composite coatings due to the facile coating fabrication and the uniformity of the deposit. Nickel matrix nano-composites by conventional electroplating [13-16] or electroless deposition [17] techniques have been widely documented in the literature. The dispersion of the nano particles plays a vital role in determining the microstructure and properties of the final composite coating. However, naturally many nano components such as Al_2O_3, SiC and carbon nanotubes (CNTs) tend to agglomerate in the plating bath, thus disturbing the current distribution and making the coating inhomogeneous. To this end, surfactants such as sodium dodecyl sulphate (SDS) and cetyl trimethylammonium bromide (CTAB) [16, 18] were often used to stabilise the composite plating solution and reduce particle agglomeration, which made the coating formula more complex.

Electro-brush plating is a modified electrodeposition technique that is highly portable and flexible [19, 20]. During the plating the brush filled with the plating solution operates against the target surface in the presence of a voltage. The brushing operation is basically a type of mechanical stirring that can smooth the coating surface and avoid the agglomerations of nano particles, even without additional surfactants. Moreover, as the deposition only occurs at the brush-article contact, much less plating solution is required, which reduces potential environment impact. Brush-plating technique has been used in the fabrication of a number of novel nano-composites; however, no report on the brush-plating of nickel-graphene composite coatings was found in the literature yet.

In this work, nickel-GO nano-composite coatings were deposited on steel using electro-

brush plating to ensure homogeneous distribution of GO sheets in the matrix. The morphology and microstructure of the obtained coatings were characterised. The mechanical properties of the composite coatings with varying GO contents were evaluated using nanoindentation. The thermal stability of some selected nickel-GO nano-composite coating was investigated by annealing at 400°C. The corrosion behaviour was investigated by means of polarisation and electrochemical impedance spectroscopy (EIS) techniques.

2. Experimental

2.1. GO synthesis

Graphene oxide (GO) was prepared based on a modified Hummers' method [21]. Briefly, one portion of graphite powder (Alfa Aesar, -325 mesh natural flakes) was mixed with six portions of potassium permanganate, and then subject to chemical reactions with a blend of chilled concentrated sulphuric acid and phosphoric acid under rigorous stirring for 12 h at 50°C. To terminate the reaction, the chocolate-coloured slurry was poured carefully onto ice, followed by the addition of 30wt% H_2O_2 solution until the mixture turned bright yellow in colour. The resulting solids, i.e. graphite oxide, were collected and then washed using copious 10wt% HCl solution and absolute ethanol in succession. To obtain a GO aqueous suspension, the dried product was dispersed and exfoliated into deionised water by ultrasonication (200 W) for 1-3 h, depending on the GO concentration.

2.2. Coating fabrication

The nickel and nickel-GO composite coatings were fabricated using a NBP-100 nano brush plating unit on which two electric poles, the workpiece and the plating pen, were attached. Type 316L stainless steel was used as the substrate material. Coupons of 20×50 mm^2 in size were ground to grit 2500, cleaned with soapy water and then degreased in acetone for 5 min under ultrasonication. A graphite rod wrapped with absorbent cotton cloth was used as the plating pen. During the plating process, the plating pen saturated with the electrolyte wiped against the steel surface at a constant speed of 10 cm/s. A voltage of 14 V was applied between

the two electrodes throughout the plating and an operation time of 30 min was adapted. The resulting sample was rinsed wish deionised water and dried in hot air.

The nickel plating solution used in this work was commercially available (Sifco ASC, part No. 2086). Nickel-GO composite plating solution was prepared by adding concentrated GO suspension dropwise into the original plating solution under continuous ultrasonication (200 W) and vigorous shaking. Four types of plating solutions with varying GO loads were prepared, and the samples from each solution were named as Ni, NG05, NG20 and NG40 according to their GO content, as listed in Table 1.

2.3. Characterisation

An atomic force microscope (AFM) in tapping mode was used to examine the morphology of the GO sheet. Raman spectra of the GO and Ni-GO composite coatings were recorded using a confocal Raman microscope (Renishaw, laser wavelength 488 nm). A field emission scanning electron microscope (FESEM, acceleration voltage 10 kV) fitted with an energy dispersive X-ray spectroscopy (EDS) accessory was employed to inspect the morphologies and chemical compositions of the coatings. X-ray diffraction (XRD) was performed within the diffraction angle range from 40° to 60° (2θ) with a step size of 0.007° and a scan speed of 0.8 second/step.

A NanoTest Vantage instrument (Micro Materials Ltd.) fitted with a Berkovich tip was used to perform nano-indentation measurements on the polished cross sections of the coatings. The maximum load, loading and unloading time were set to be 10 mN, 30 s and 30s, respectively. The corrosion behaviour of the coatings in a 3.5wt.% NaCl solution was investigated by means of potentiodynamic polarisation and electrochemical impedance spectroscopy (EIS) using a Gamry Interface 1000 potentiostat. A platinum counter electrode and a saturated calomel reference electrode (SCE) were used. The open circuit potential (OCP) of the sample was recorded for 1 h before the following measurements. The polarisation measurements were performed in the range of -0.2 to +1.0 V (versus the finishing OCP) at a scan rate of 1 mV/s.

The impedance was measured over a frequency range of 10m – 100k Hz with a sinusoidal voltage amplitude of 10 mV.

3. Results

3.1 Morphology and microstructure

Figure 1 shows the morphology of the obtained GO sheets under AFM. The similar contrast between the planar sheets and the background (a silicon wafer) indicates a uniform thickness of the exfoliated GO sheets. The height profile across an individual GO sheet revealed a thickness of approximately 1 nm, suggesting that the GO sheets are single-layer.

Four coatings, i.e. Ni, NG05, NG20 and NG40 were prepared by brush plating under the same plating conditions and their morphologies are compared in Figures 2a-d. It is a clear trend that the surface roughness of the resulting coatings increased with increasing GO load. The neat (i.e. GO-free) nickel coating (Figure 2a) appeared to be compact and smooth, with few bumps and pin holes. The addition of 0.5 mg/ml GO into the plating solution resulted in the formation of nodules on the coating surface, together with some areas of clusters as circled in Figure 2b. As the GO concentration increased to 2.0 mg/ml, the nodules observed on coating NG20 (Figure 2c) became finer in size but higher in density. A further increase of the GO concentration to 4.0 mg/ml led to large surface fluctuation with a dense yet uniform distribution of agglomerations, as demonstrated in Figure 2d. The change in topography is believed to be caused by the introduction of GO. Figure 2e is a typical enlarged view of the Ni-GO composite coatings that was observed at some defect sites as pointed out in Figure 2c and at the agglomerations showed in Figures 2b and 2d. The nickel clusters were all netted by ubiquitous translucent thin membranes, which is characteristic of graphene and graphene oxide sheets under SEM [22, 23].

Raman spectra of the original GO sheets and three Ni-GO composite coatings NG05, NG20 and NG40, were recorded and shown in Figure 2f. All the spectra display two bands around 1350 and 1600 cm^{-1}, which are characteristic of many carbonaceous materials. The G band around 1600 cm^{-1} represents the intrinsic sp^2-conjugated structure of graphene, while the

D band around 1350 cm^{-1} rose in the presence of structural defects and disorders in the carbon skeleton. The intensity ratio of D band to G band (I_D/I_G) is therefore usually used as an indicator of the disorder degree in graphene. The calculated I_D/I_G ratios for NG05, NG20 and NG40 are 0.86, 0.88 and 0.84, respectively, which are both higher than that (0.71) of the original GO. This increase in the I_D/I_G ratio for the Ni-GO composite coatings is a reflection of the increased disorder degree as mentioned above. This could be attributed to the distortion of the GO sheets among the nickel grains, and more likely the absorption or chemical bonding of nickel ions during the coating formation that could have introduced more defects and reduced the average size of the sp^2 domains in the graphene structure [24].

To evidence the incorporation of GO into the Ni-GO composite coatings developed, cross-sectional fractures of both neat nickel coating and a Ni-GO composite coating were prepared and compared in Figure 3. Without any GO addition to the brush plating solution, the cross-section of the resulted coating appeared to be layer-structured (Figure 3a), which is consistent with the observations on such coatings in the literature [25, 26]. This Ni coating showed a thickness of approximately 6 μm after plating for 30 min. In comparison, the Ni-GO composite coating (Figure 3b) exhibited prominent turbulence in terms of the layered structure. This is likely due to the GO sheets that wrapped and intersected the nickel clusters and thus disturbed the normal crystallisation process. It should also be noted that with the same working voltage and operation time the thickness of the Ni-GO composite coating measured to be about 4 μm, around 1/3 thinner than that of the neat Ni coating. Figures 3c-d provide details of the fractography of the composite coating under higher magnifications. Note that the cross-section was subject to mild argon plasma milling before SEM in order to enhance the presentation. It can be seen clearly that the thin semi-transparent sheets (GO) were embedded between nickel crystals (or vice versa) and conformed the contours of the nickel clusters well.

EDS analysis was performed on the cross-section of each coating with the result demonstrated in Figure 3e. Compared with the neat Ni coating, a relatively higher content of

carbon (5.37 vs 2.15, wt.%) was detected from the NG coating although it is known that EDS is not an accurate method for quantitative measurement of such light element as carbon. The microscopical observation and elemental analysis confirm that GO sheets not only exist near the surface, but have also been incorporated into the bulk matrix successfully.

The XRD patterns of neat Ni and Ni-GO composite coatings (NG05, NG20 and NG40) are presented in Figure 4. All three patterns exhibit a prominent peak around 44° and another peak at ~51.5° which correspond to the (111) and (200) crystallographic planes of nickel, respectively. As seen in the plot, the (111) peak was broadened and the (200) peak attenuated as GO was introduced into the matrixes, implying a possible grain size reduction promoted by the incorporated GO. To this end, the average crystallite sizes of the coatings were estimated using Scherrer equation as below:

$$\beta = \frac{K\lambda}{L\cos\theta} \cdot \frac{180^\circ}{\pi} \quad (1)$$

where β is the full width half maxima (FWHM) of the (111) diffraction in 2θ degree, K is Scherrer constant (0.94 used here), λ is the wavelength of Cu-K_α radiation (0.154 nm), θ is the diffraction angle, L is the crystallite size in nm. In light of possible instrumental broadening and microstrain in the matrixes, the calculated values were normalised and compared in Table 2. In particular, the average grain size for NG40 was about 40% smaller than the neat Ni coating, suggesting a significant refinement.

3.2. Mechanical properties

Nanoindentation tests were carried out on both neat Ni and Ni-GO composite coatings (NG05, NG20 and NG40) at a fixed peak load of 10 mN. To minimise the influence of the coating thickness and surface roughness, the measurements were performed on the polished cross-sections. Typical loading-unloading curves for each sample were presented in Figure 5. It can be seen that the Ni-GO composite coatings showed less indentation depths than the neat Ni at both the maximum and final stages, indicating their improved indentation resistance. As the GO content (concentration in the plating solution) increased from 0 to 2.0 mg/ml, the

indentation maximum was reduced by ~25 nm, due to the improved hardness. This enhancement is likely related to the grain size reduction after the inclusion of GO nano sheets, as well as the inherent high mechanical properties of GO. However, NG40 exhibited a 'softening' effect compared with the other two composite coatings. This phenomenon may be the result of fine yet defective microstructure of NG40. Nonetheless, it is worth noting that the hardness of NG40 was still higher than that of the neat Ni coating.

The nanoindentation hardness and reduced modulus (E_r) were calculated from the loading-displacement curves based on the Oliver-Pharr fit [27]. The results are summarised in Table 3. The hardness and reduced modulus of the nano-composite coatings were improved by up to 0.9 GPa and 20 GPa respectively with GO addition until NG40 where a drop in both hardness and elastic modulus was observed. The unexpected drop in the NG40 case indicates that a too high GO concentration in the plating solution might have led to degraded mechanical properties of the resulting composite coating.

Plasticity index (PI) is a parameter usually used to evaluate the elastic-plastic response of a material to external applied forces. In nanoindentation, the PI of the tested material can be characterised by the area included in the load-displacement curve (non-reversible plastic work) using the following equation:

$$\psi = \frac{A_1 - A_2}{A_1} \quad (2)$$

where ψ is the plasticity index, A_1 and A_2 are the areas under the loading curve (total work) and unloading curve (elastic work), respectively. The calculated PI values for each sample are listed in Table 3. Interestingly, all the three GO-containing coatings exhibited lower plasticity than the GO-free nickel coating, including NG40 which showed the highest reduction of ~8% towards the plasticity index. This is in line with the observation in Figure 5 that all the Ni-GO composite coatings left a smaller final indentation depth, regardless of the increased peak depth in the NG40 case.

More interestingly, preliminary study (unpublished) has revealed that GO improved the

thermal stability of the Ni-GO composite coatings effectively. The GO-containing nickel coating exhibited less degradation in mechanical strength when annealed at elevated temperatures. After kept at 400 °C for 30 min, for example, the hardness of the neat Ni coating was reduced by 30% (7.75 GPa to 5.5 GPa), while in sharp contrast the NG20 composite coating remained nearly no change in hardness (8.65 GPa to 8.63 GPa). The detailed investigation shall be reported somewhere when completed.

3.3 Corrosion behaviour

Corrosion behaviour of the brush-plated Ni-GO nano-composite coatings (NG05, NG20 and NG40) as well as the neat Ni coating was investigated by means of polarisation and EIS measurements in a 3.5wt.% NaCl solution. Figure 6 shows the polarisation curves after an OCP measurement for 1 h. In comparison to the neat Ni coating, both NG20 and NG40 demonstrated a clear positive shift of the corrosion potential (E_{corr}), revealing a less corrosion tendency. NG05 showed marginal shift in E_{corr} due to the small amount of incorporation. The results of Tafel fit to the polarisation curves (Table 4) also display that in the presence of GO fillers the corrosion current densities (I_{corr}) of NG20 and NG40 decreased remarkably by approximately 60% and 70%, respectively. Accordingly, the corrosion rate was suppressed down to 55.8 $\times 10^{-3}$ mpy (NG20) and 39.3 $\times 10^{-3}$ mpy (NG40) from the 131.4 $\times 10^{-3}$ mpy for the GO-free coating. NG20 demonstrated a passive characteristic within a wide range of the anodic polarisation period (from E_{corr} to ~0 V vs. SCE), indicating an enhanced impermeability owing to the GO sheets. A breakdown point at ~0 V was met, after which the polarisation current built up quickly to a high level equal to the neat Ni, suggesting that the GO components lost their power in preventing the corrosive electrolyte from penetrating through the coating. NG40 resembled NG20 roughly in terms of the polarisation curve shape, whilst exhibiting a slightly more negative corrosion potential and higher current densities in the anodic polarisation section, indicating a smaller polarisation resistance. The turbulences of the anodic polarisation currents occurred on some of the tested samples and could be related to solvent penetration through the

localised defects within the nickel matrixes.

To elucidate the corrosion protection mechanism for each type of coating, electrochemical impedance spectroscopy (EIS) measurements were carried out on neat Ni, NG05, NG20 and NG40. In EIS, a small sinusoidal electrical signal (±10 mV, 10m – 100k Hz in this work) about the open circuit potential is applied to the sample surface and the electrochemical response to the excitation at different frequencies is recorded and analysed [28]. Figure 7a is the Bode plot in which the absolute values of the impedance (|Z|) and the phase angle are plotted as the function of excitation frequency. At the highest frequencies the |Z| magnitude plots are flat, revealing primarily the resistance of the electrolyte solution (R_s). At intermediate frequencies, the capacitive response from the coating system (C_c) predominates, which is characterised by diagonal lines in the |Z| magnitude plots and the largest phase angles. As the frequency is further lowered, the coating resistance R_c (or interfacial charge transfer resistance R_{ct}) tends to dominate the total impedance, depicted by flattened |Z| curves as resistors are independent of frequency. It is revealed in Figure 7a that the impedance moduli |Z| of NG20 and NG40 at the lowest frequency were both significantly higher than that of the neat Ni, which is a sign of higher corrosion resistance. The |Z| plots of NG05 and NG40 largely resembled that of NG20, until around the lowest frequency end when the impedance moduli headed down to some extent.

Figure 7b displays the corresponding Nyquist plots for the tested samples, in which the impedance at each frequency is located according to its real (resistive) and imaginary (capacitive) components. NG05 showed a dataset similar to that of neat Ni. NG20 and NG40 coatings showed remarkably larger semi-circular arc compared with the neat Ni coating. In general, a larger impedance arc is the result of a higher polarisation (or electron charge transfer) resistance, and much likely a reflection of a greater corrosion resistance. It is also worth noting that the NG40 exhibited an unusual impedance loop at low frequencies (the far end of the impedance arc). This loop is related to an inductive behaviour rather than capacitive, which could be ascribed to the corrosion and dissolution of the metallic surface and the adsorption of

the intermediate species [29].

In order to quantify the interpretation of the EIS spectra, electrical equivalent circuit models of the three corrosion systems were attempted. The adapted model and corresponding fitting curves (solid lines) are illustrated in Figure 7b and the refined fit parameters for each coating sample summarised in Table 5. A constant phase element (CPE) is a circuit element with a constant phase shift over the frequency, and was employed in this work to model an imperfect capacitor, whose impedance is expressed as:

$$Z_{CPE}(\omega) = \frac{1}{CPE \cdot (j\omega)^n} \quad (3)$$

where n is the phase shift index (n=1 for an ideal capacitor). R_s, R_c and CPE_C (C_C) were employed as previously described. An additional pair of double layer capacitance (CPE_{dl}) and charge transfer resistance (R_{ct}) were introduced in order to simulate the situation where the electrolyte penetrates into the coating and forms a new electric double layer at the liquid/metal interface. It is revealed in Table 5 that the R_c for the neat Ni coating was just 6.8 kΩ·cm^2, while NG20 and NG40 exhibited a dramatically increased R_c of 519 kΩ·cm^2 and 371 kΩ·cm^2, respectively, indicative of a much greater resistance to the corrosion environment. Furthermore, their higher R_{ct} and CPE_{dl} values suggest that the two coatings were less permeable owing to the presence of GO sheets, thus exposing less active area to the corrosive electrolyte, and thus corrosion was less likely. Similar increase in R_{ct} was also reported by Park et al. [30] and Zhou et al. [31]. The overall polarisation resistance (R_c + R_{ct}) increases in the order of Ni (118 kΩ·cm^2) < NG05 (133 kΩ·cm^2) < NG40 (548 kΩ·cm^2) < NG20 (678 kΩ·cm^2).

4. Discussion

4.1. The successful incorporation of GO in the nickel matrix

The current study explored the use of electro-brush plating for the fabrication of a nickel-graphene oxide nano-composite coating. Several characterisation methods, such as top-view and cross-sectional SEM observation, EDS, Raman as well as XRD were employed to confirm

the successful incorporation of GO sheets which was not only at the surface but also deep into the nickel matrixes. Due to their flexibility and high aspect ratio, GO sheets were able to fit in small corners and caves and wrap nickel clusters of whatever sizes during the coating fabrication, as evidenced in Figure 2e, Figures 3c-d and Figure 8c. It is likely that in the final composite matrix the ultrathin GO sheets were entangled and cross linked with each other and appear as a high-density 3D network architecture in which nickel grains nucleate, grow and connect. In addition, due to the hydrolysis of the oxygen functional groups (in particular the –COOH carboxyl groups) on the GO structure, a GO sheet can readily show negative charges in water. Thus, it is plausible that nickel cations show a high affinity to GO sheets and tend to settle down on them. Meanwhile, it has been reported that GO can be electrochemically reduced (and thus form rGO) at a very small negative potential [32], via cyclic voltammetry sweeping [33-35] or during electroplating [15]. In this study, the voltage applied between the brush (anode) and the substrate (cathode) during coating fabrication was 14 V. Although the exact value of the potential applied on the cathode is difficult to monitor due to technical reasons, as a potential of -1 V to -2 V is enough to initiate the electrochemical reduction of GO [32], it is believed that the GO sheets in the nickel matrixes might have been reduced. To this end, XPS analysis of the as-prepared GO and the resultant Ni-GO composite were performed. Figure 9 compares the C1s spectra of the two samples. The Ni-GO composite showed significant attenuated C-O and C=O peaks compared to as-prepared GO, indicating a remarkable reduction effect during the coating deposition. Once nickel ions attach to the surface of rGO sheets they can be instantly reduced to metallic nickel owing to the electrical conductivity of rGO, which enables quick electron transfer from the substrate (cathode). In other words, GO incorporation promoted the nucleation process of nickel ions. This is evidenced in this work by the observation that fine nickel spheres formed on GO sheets (Figure 8a). It is also echoed by Zhang et al. [24] who demonstrated the fabrication of Ni ion decorated GO making use of the chemical activity of GO.

The reduced coating thickness after introducing GO as compared in Figure 3 could be two-fold. On one hand, it could be a result of the lower deposition efficiency from the GO-containing plating solution. As discussed in the preceding paragraph, the GO sheets were reduced electrochemically at the cathode during deposition, thus consuming a fraction of the current efficiency and leading to a lower deposition rate for nickel. On the other hand, it could also be ascribed to the increased viscosity of the plating solution with increasing GO load due to the very high aspect ratio of GO sheets. As basically it is a liquid-based deposition technique, the deposition rate would decrease if the plating solution became thicker. Actually, at a GO concentration of 6 mg/ml, all the attempts to obtain a coating from the plating slurry failed.

There have been a number of reports on the electrodeposition of Ni-graphene composites and the majority of them are about conventional electroplating [15, 31, 36-39]. In the available reports, a small GO load of 0.05-2 mg/ml was commonly used, while the obtained coatings usually showed rough morphology due to the agglomerations of GO sheets [37-39]. To the best of our awareness, there is no any report yet on the brush-plating of such nano-composite coatings. One of the biggest advantages of brush plating over conventional electrodeposition techniques is that the former enables higher nano filler load (up to 4 mg/ml in this work) into the matrix while smoothing the coating surface owing to the use of an additional mechanical force during the plating process. As shown in Figure 2, the electro-brush plated Ni-GO coatings possess low surface roughness. For comparison, Figure 10 displays the morphology of a Ni-GO composite coating by conventional electroplating with a GO load of 0.5 mg/ml. Around the bulges it showed well-defined crystals, which was pure nickel (GO-free) by EDS analysis. A large number of carbon-rich bulges formed on the coating surface, which is consistent with the literature on similar composites [39].

4.2. Microstructure – mechanical property relationship

It has been demonstrated by means of XRD that the average crystallite sizes of the GO-containing composite coatings were smaller, which could be associated with the nucleation

promotion effect of GO as discussed above. In an electrochemical deposition process the nucleation and crystal growth compete against each other [37], i.e. the higher the nucleation rate, the smaller the grown crystals could be. Moreover, it was evidenced by SEM (see Figure 8b) that GO sheets intersected the nickel clusters randomly, thus obstructing the normal growth of the nickel crystals and providing nucleation sites for new grains [40]. Based on the discussion above, the grain size refinement could be explained.

With regards to mechanical properties, it is well known that grain size refining is among the main ways for the strengthening of a material. Thus, the improved hardness and Young's modulus of the Ni-GO composite coating could be associated with the reduced grain size of the matrix (Table 2). Moreover, the incorporated graphene oxide sheets could demonstrate an anchor effect which prevented nickel grains from sliding, thus enhancing the mechanical properties [10, 40]. Additionally, the intrinsic mechanical strength of graphene oxide might have a contribution to the enhancement of the Ni-GO composite coatings. While pristine graphene possesses a Young's modulus of 1 TPa and an intrinsic strength of 130 GPa [2], it is reported that the mechanical properties of a graphene sheet are inversely affected by the degree of structural defects, such as holes, vacancies and oxygen functional groups [41]. AFM tip indentation experiments showed effective Young's moduli of 207.6±23.4 GPa, 223.9±17.7 GPa and 229.5±27.0 GPa for monolayer, bilayer and three-layer GO, respectively [42]. After reduction, rGO monolayers showed a Young's modulus of 250 GPa [43]. Given that the GO sheets in the nickel matrixes in this work have been reduced as discussed in Section 4.1, the elastic modulus of the incorporated GO sheets should fall between the reported values for GO (~200 GPa) and rGO (~250 GPa), either of which is higher than that of the neat Ni (~185 GPa, see Table 3) in this work. Improvements of the mechanical properties of the resultant composites can thus be expected.

However, when the GO content is beyond a specific level (for instance, NG40 in this work) agglomeration is likely to occur, which may lead to more defects and ultimately result in

a reduced hardness [44]. Nevertheless, the NG40 composite coating was still able to show an improved resistance to plastic deformation, much likely due to the inherent strength of the cross-linked GO sheets.

4.3. Effect of GO on the corrosion resistance of the composite coating

The impermeability of the GO structure is believed to be the origin for the improvement in corrosion resistance of the Ni-GO composite coatings. Although only one-atom-thick, graphene can block all molecules including helium the smallest from passing through [45]. The chloride ions (Cl^-) whose van der Waals diameter is 0.35 nm are much larger than the pore size (0.064 nm) on the carbon network of graphene oxide, which means GO can act as an extraordinary physical barrier against corrosive species [3]. Given the limited dimensions of a GO sheet, it seems that the edges of the GO sheets as well as the micro voids/defects generated within the nickel matrixes were the possible passages for the electrolyte. Therefore, the interaction between the GO sheets and the nickel matrix is of much importance for the anti-corrosion performance.

Brush-plated Ni coatings naturally contain a more or less number of voids and pin holes [25, 26], leading to an unstable electrolyte/coating interface due to transient penetration of water and corrosive species (mainly Cl^-) via these defects. As a result, the electrochemical interface area would increase and so the total corrosion current flow. This is consistent with the observation of sparkles in the anodic polarisation curves of the neat Ni and NG40 (Figure 6). However, unlike the common pitting featuring catastrophic increase of the corrosion current, the pittings in Figure 6 were metastable and stopped by re-passivation of the interior of the voids and pinholes. In such a circumstance, a low coating resistance R_c but a relatively high capacitance CPE_c for the neat Ni coating were measured as the pinholes were filled with electrolyte which largely increased the ion conductivity and dielectric constant. As the internal area exposed to the electrolyte accumulated, it could also be expected that an electric double layer formed at the electrolyte/metal interface, modelled by a double layer capacitance (CPE_{dl})

and charge transfer resistance (R_{ct}) as seen in Figure 7b. It is worth noting that unlike organic coating systems where the CPE_{dl} and R_{ct} are usually allocated at the coating/metal substrate interface, in this case the electric double layer could be formed at the GO/Ni interface within the coating, too. Given these information, the remarkable increase in R_c and the depressed CPE_c for both GO-containing coatings could be attributed to the excellent barrier effect of GO which inhibited the water uptake effectively. In the meantime, GO could have reduced the chemical activities for electrolyte/Ni and electrolyte/substrate interfaces, suggested by the higher R_{ct} and CPE_{dl}. The corrosion behaviour of the electro-brush plated composite coatings outperformed those by conventional electroplating. For example, the EIS results showed an improvement of 2 times [39] and 1.5 times [31] in cases of electroplated Ni-graphene (oxide) composite coatings, while in this study the corrosion impedance of NG20 was remarkably 6 times larger than neat Ni.

With reference to NG40, the negative shift in corrosion potential, higher current density and the degraded EIS data set in comparison with NG20 might be related to a loose and defective microstructure which let more electrolyte in than NG20. This is in line with the findings from the XRD and mechanical measurements that NG40 was weaker in terms of its mechanical strength in spite of its reduced grain size. It has been reported that the graphene or carbon nanotube (CNT) fillers inside a metallic matrix even promoted the corrosion at the carbon/metal interface in the presence of electrolyte, as graphene and CNT are chemically nobler than the coating metals [46, 47]. Therefore, it is essential to enhance the interaction between the nano fillers and the matrix for a good mechanical and anti-corrosion performance.

5. Conclusion

In conclusion, an electro-brush plating technique was employed in this work for the novel fabrication of a nickel-graphene oxide (GO) nano-composite coating and the effect of GO on the mechanical and anti-corrosion properties of the composite coating was investigated. The characterisation results confirm that GO sheets have been incorporated into the nickel matrix

successfully. The brush plating method is beneficial for the fabrication of the nano-composite as it allowed a high GO load yet compact and smooth coating morphology. It was shown by XRD that the average crystallite size of the nickel matrix can be considerably reduced by introducing GO sheets. The nanoindentation and electrochemical studies have revealed that GO nano fillers of a proper content can effectively improve the hardness, Young's modulus, thermal stability and corrosion resistance. The improvement in mechanical properties both at room temperature and elevated temperatures could be mainly attributed to the grain refining and pinning effect of the GO nano sheets. The enhanced anti-corrosion performance can be associated with the excellent physical barrier effect of the GO sheets. However, excessive GO can be detrimental to both mechanical properties and corrosion resistance of the composite coating. Thus, the GO load in the composite needs to be tuned with care and it is worth investigating the varied microstructures in more details.

Acknowledgements

This work was financially supported by EU H2020 MODCOMP project [Contract No. 685844]. One of the authors (SQ) wishes to express his appreciation to China Scholarship Council (CSC) and The University of Birmingham & School of Metallurgy and Materials for the PhD studentship.

References

[1] K.S. Novoselov, V.I. Fal'ko, L. Colombo, P.R. Gellert, M.G. Schwab, K. Kim, A roadmap for graphene, Nature 490 (2012) 192-200.

[2] C. Lee, X. Wei, J.W. Kysar, J. Hone, Measurement of the elastic properties and intrinsic strength of monolayer graphene, Science 321 (2008) 385-388.

[3] V. Berry, Impermeability of graphene and its applications, Carbon 62 (2013) 1-10.

[4] H. Dong, S. Qi, Realising the potential of graphene-based materials for biosurfaces – A future perspective, Biosurf. Biotribol. 1 (2015) 229-248.

[5] D. Prasai, J.C. Tuberquia, R.R. Harl, G.K. Jennings, K.I. Bolotin, Graphene- Corrosion-inhibiting coating, ACS nano 6 (2012) 1102-1108.

[6] Y. Su, V.G. Kravets, S.L. Wong, J. Waters, A.K. Geim, R.R. Nair, Impermeable barrier films and protective coatings based on reduced graphene oxide, Nat. Commun. 5 (2014).

[7] T. Kuila, S. Bose, A.K. Mishra, P. Khanra, N.H. Kim, J.H. Lee, Chemical functionalization of graphene and its applications, Prog. Mater. Sci. 57 (2012) 1061-1105.

[8] S. Stankovich, D.A. Dikin, G.H. Dommett, K.A. Kohlhaas, E.J. Zimney, E.A. Stach, R.D. Piner, S.T. Nguyen, R.S. Ruoff, Graphene-based composite materials, Nature 442 (2006) 282-286.

[9] Y. Liu, Z. Dang, Y. Wang, J. Huang, H. Li, Hydroxyapatite/graphene-nanosheet composite coatings deposited by vacuum cold spraying for biomedical applications: Inherited nanostructures and enhanced properties, Carbon 67 (2014) 250-259.

[10] A. Dorri Moghadam, E. Omrani, P.L. Menezes, P.K. Rohatgi, Mechanical and tribological properties of self-lubricating metal matrix nanocomposites reinforced by carbon nanotubes (CNTs) and graphene – A review, Compos. Part B Eng. 77 (2015) 402-420.

[11] C. Min, P. Nie, H.-J. Song, Z. Zhang, K. Zhao, Study of tribological properties of polyimide/graphene oxide nanocomposite films under seawater-lubricated condition, Tribol. Int. 80 (2014) 131-140.

[12] B. Szczygieł, M. Kołodziej, Composite Ni/Al2O3 coatings and their corrosion resistance, Electrochim. Acta 50 (2005) 4188-4195.

[13] T. Borkar, S.P. Harimkar, Effect of electrodeposition conditions and reinforcement content on microstructure and tribological properties of nickel composite coatings, Surf. Coat. Tech. 205 (2011) 4124-4134.

[14] C.K. Lee, Wear and corrosion behavior of electrodeposited nickel–carbon nanotube composite coatings on Ti–6Al–4V alloy in Hanks′ solution, Tribol. Int. 55 (2012) 7-14.

[15] Z. Ren, N. Meng, K. Shehzad, Y. Xu, S. Qu, B. Yu, J.K. Luo, Mechanical properties of nickel-graphene composites synthesized by electrochemical deposition, Nanotechnology 26 (2015) 065706-065711.

[16] C. Guo, Y. Zuo, X. Zhao, J. Zhao, J. Xiong, Effects of surfactants on electrodeposition of

nickel-carbon nanotubes composite coatings, Surf. Coat. Tech. 202 (2008) 3385-3390.

[17] J. Sudagar, J. Lian, W. Sha, Electroless nickel, alloy, composite and nano coatings – A critical review, J. Alloy. Compd. 571 (2013) 183-204.

[18] E. Rudnik, L. Burzyńska, Ł. Dolasiński, M. Misiak, Electrodeposition of nickel/SiC composites in the presence of cetyltrimethylammonium bromide, Appl. Surf. Sci. 256 (2010) 7414-7420.

[19] B. Wu, B.-s. Xu, B. Zhang, X.-d. Jing, C.-l. Liu, Automatic brush plating: An update on brush plating, Mater. Lett. 60 (2006) 1673-1677.

[20] G. Ma, B. Xu, H. Wang, X. Wang, G. Li, S. Zhang, Research on the microstructure and space tribology properties of electric-brush plated Ni/MoS2–C composite coating, Surf. Coat. Tech. 221 (2013) 142-149.

[21] D.C. Marcano, D.V. Kosynkin, J.M. Berlin, Improved synthesis of graphene oxide, ACS nano 4 (2010) 4806-4814.

[22] S. Mayavan, T. Siva, S. Sathiyanarayanan, Graphene ink as a corrosion inhibiting blanket for iron in an aggressive chloride environment, RSC Adv. 3 (2013) 24868-24871.

[23] M.-S. Wu, Y.-P. Lin, C.-H. Lin, J.-T. Lee, Formation of nano-scaled crevices and spacers in NiO-attached graphene oxide nanosheets for supercapacitors, J. Mater. Chem. 22 (2012) 2442-2448.

[24] H. Zhang, X. Zhang, D. Zhang, X. Sun, H. Lin, C. Wang, Y. Ma, One-step electrophoretic deposition of reduced graphene oxide and Ni(OH)2 composite films for controlled syntheses supercapacitor electrodes, J. Phys. Chem. B 117 (2013) 1616-1627.

[25] B. Xu, H. Wang, S. Dong, B. Jiang, Fretting wear-resistance of Ni-base electro-brush plating coating reinforced by nano-alumina grains, Mater. Lett. 60 (2006) 710-713.

[26] W.-h. Li, X.-y. Zhou, Z. Xu, M.-j. Yan, Microstructure of Ni–polytetrafluoroethylene composite coating prepared by brush electroplating, Surf. Coat. Tech. 201 (2006) 1276-1281.

[27] W.C. Oliver, G.M. Pharr, An improved technique for determining hardness and elastic modulus using load and displacement sensing indentation experiments, J. Mat. Res. 7 (1992) 1564-1583.

[28] R.G. Kelly, J.R. Scully, D.W. Shoesmith, R.G. Buchheit, Electrochemical techniques in corrosion science and engineering, Marcel Dekker, Inc., USA, 2003.

[29] F.H. Cao, Z. Zhang, J.X. Su, J.Q. Zhang, Electrochemical impedance spectroscopy analysis on aluminum alloys in EXCO solution, Mater. Corros. 56 (2005) 318-324.

[30] J.H. Park, J.M. Park, Electrophoretic deposition of graphene oxide on mild carbon steel for anti-corrosion application, Surf. Coat. Tech. 254 (2014) 167-174.

[31] P. Zhou, W. Li, Y. Li, X. Lu, X. Jin, J. Chen, Fabrication and Corrosion Performances of Pure Ni and Ni-Based Coatings Containing Rare Earth Element Ce and Graphene by Reverse Pulse Electrodeposition, J. Electrochem. Soc. 164 (2017) D75-D81.

[32] X.-Y. Peng, X.-X. Liu, D. Diamond, K.T. Lau, Synthesis of electrochemically-reduced

graphene oxide film with controllable size and thickness and its use in supercapacitor, Carbon 49 (2011) 3488-3496.

[33] M. Zhou, Y. Wang, Y. Zhai, J. Zhai, W. Ren, F. Wang, S. Dong, Controlled synthesis of large-area and patterned electrochemically reduced graphene oxide films, Chemistry 15 (2009) 6116-6120.

[34] J. Molina, J. Fernández, A.I.D. Río, J. Bonastre, F. Cases, Synthesis of Pt nanoparticles on electrochemically reduced graphene oxide by potentiostatic and alternate current methods, Materials Characterization 89 (2014) 56-68.

[35] L. Chen, Y. Tang, K. Wang, C. Liu, S. Luo, Direct electrodeposition of reduced graphene oxide on glassy carbon electrode and its electrochemical application, Electrochemistry Communications 13 (2011) 133-137.

[36] C.M.P. Kumar, T.V. Venkatesha, R. Shabadi, Preparation and corrosion behavior of Ni and Ni–graphene composite coatings, Mater. Res. Bull. 48 (2013) 1477-1483.

[37] H. Algul, M. Tokur, S. Ozcan, M. Uysal, T. Cetinkaya, H. Akbulut, A. Alp, The effect of graphene content and sliding speed on the wear mechanism of nickel–graphene nanocomposites, Appl. Surf. Sci. 359 (2015) 340-348.

[38] D. Kuang, L. Xu, L. Liu, W. Hu, Y. Wu, Graphene–nickel composites, Appl. Surf. Sci. 273 (2013) 484-490.

[39] K. Jiang, J. Li, J. Liu, Electrochemical codeposition of graphene platelets and nickel for improved corrosion resistant properties, RSC Adv. 4 (2014) 36245-36252.

[40] T. Borkar, S. Harimkar, Microstructure and wear behaviour of pulse electrodeposited Ni–CNT composite coatings, Surf. Eng. 27 (2011) 524-530.

[41] Q. Zheng, Z. Li, Y. Geng, S. Wang, J.-K. Kim, Molecular dynamics study of the effect of chemical functionalization on the elastic properties of graphene sheets, J. Nanosci. Nanotechnol. 10 (2010) 7070-7074.

[42] J.W. Suk, R.D. Piner, J. An, R.S. Ruoff, Mechanical properties of monolayer graphene oxide, ACS nano 4 (2010) 6557-6564.

[43] C. Gómez-Navarro, M. Burghard, K. Kern, Elastic properties of chemically derived single graphene sheets, Nano Letters 8 (2008) 2045-2049.

[44] L.Y. Wang, J.P. Tu, W.X. Chen, Y.C. Wang, X.K. Liu, C. Olk, D.H. Cheng, X.B. Zhang, Friction and wear behavior of electroless Ni-based CNT composite coatings, Wear 254 (2003) 1289-1293.

[45] J.S. Bunch, S.S. Verbridge, J.S. Alden, A.M. van der Zande, J.M. Parpia, H.G. Craighead, P.L. McEuen, Impermeable atomic membranes from graphene sheets, Nano lett. 8 (2008) 2458-2462.

[46] W. Sun, L. Wang, T. Wu, M. Wang, Z. Yang, Y. Pan, G. Liu, Inhibiting the corrosion-promotion activity of graphene, Chem. Mater. 27 (2015) 2367-2373.

[47] S.-K. Kim, T.-S. Oh, Electrodeposition behavior and characteristics of Ni-carbon nanotube composite coatings, Trans. Nonferrous Met. Soc. China 21 (2011) s68-s72.

List of figure captions

Figure 1. AFM image of the obtained graphene oxide (GO) and the height profile (black curve) of a GO sheet.

Figure 2. Morphologies of (a) neat Ni and (b-e) Ni-GO composite coatings. (f) compares the Raman spectra of GO sheets and two Ni-GO composite coatings.

Figure 3. Cross-sectional view of (a) neat Ni coating and (b-d) Ni-GO composite coatings. (e) displays the EDS spectra collected from the fractures of the neat Ni and the NG coatings.

Figure 4. XRD patterns of neat Ni, NG05, NG20 and NG40 coatings.

Figure 5. Typical load-displacement curves of the nanoindentation tests at a fixed peak load of 10 mN on (a) neat Ni, (b) NG05, (c) NG20 and (d) NG40 coatings.

Figure 6. Polarisation curves of (a) neat Ni, (b) NG05, (c) NG20 and (d) NG40 coatings in a 3.5wt.% NaCl solution.

Figure 7. (a) Bode and (b) Nyquist plots for different samples in a 3.5wt.% NaCl solution. The inserted plot in (b) is the equivalent circuit model proposed for the coating system. The dots and the solid lines in (b) illustrate the original impedance data and the fitted curves, respectively.

Figure 8. (a) Surface of a Ni-GO composite coating showing nickel crystalline spheres grown on GO sheets. (b) Nickel grains intersected by a GO sheet. (c) enlarged view of the coating cross-section, showing the nickel grains embraced by GO sheets.

Figure 9. XPS C1s spectra of (a) as-prepared GO and (b) Ni-GO composite coating.

Figure 10. SEM image showing the high degree of GO agglomeration of the composite coating by conventional electroplating.

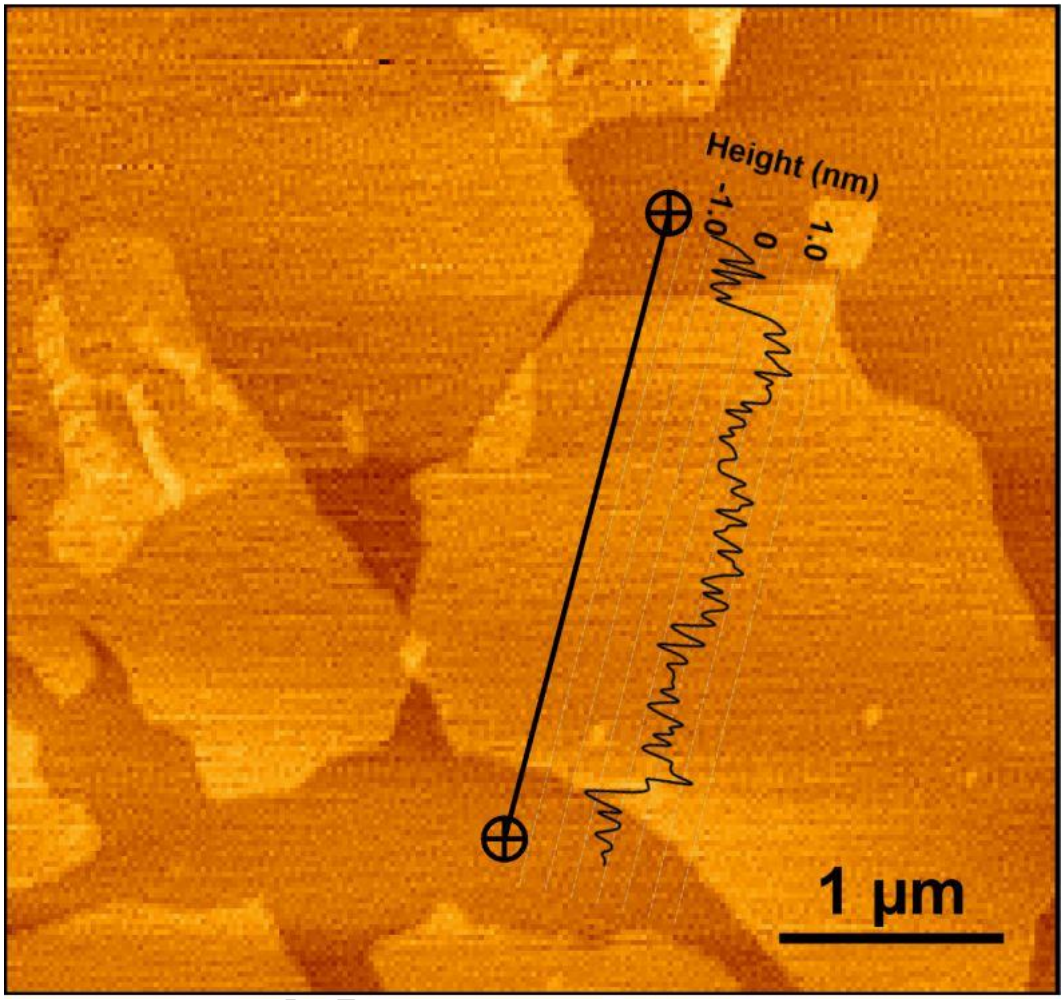

Figure 1

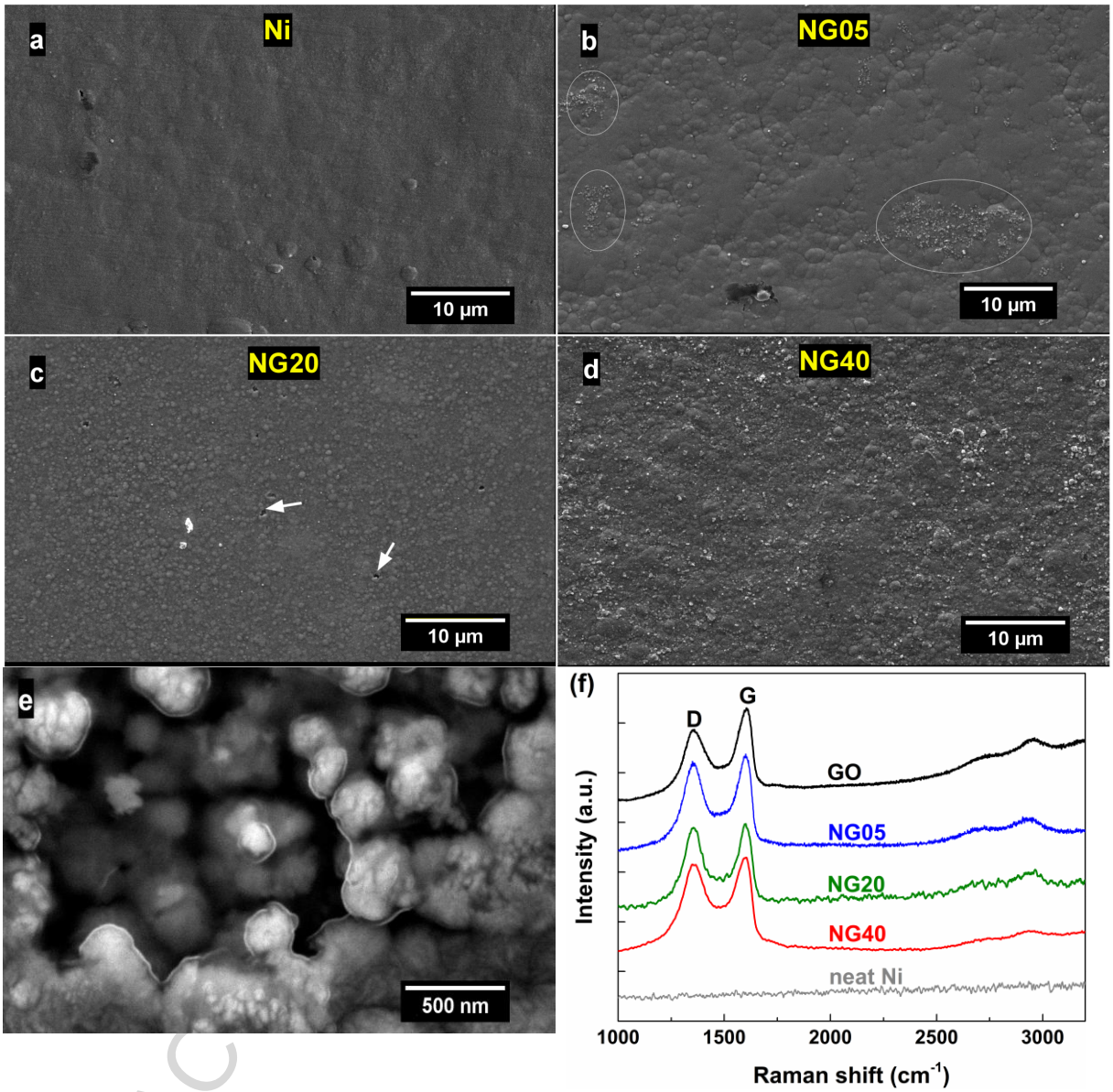

Figure 2

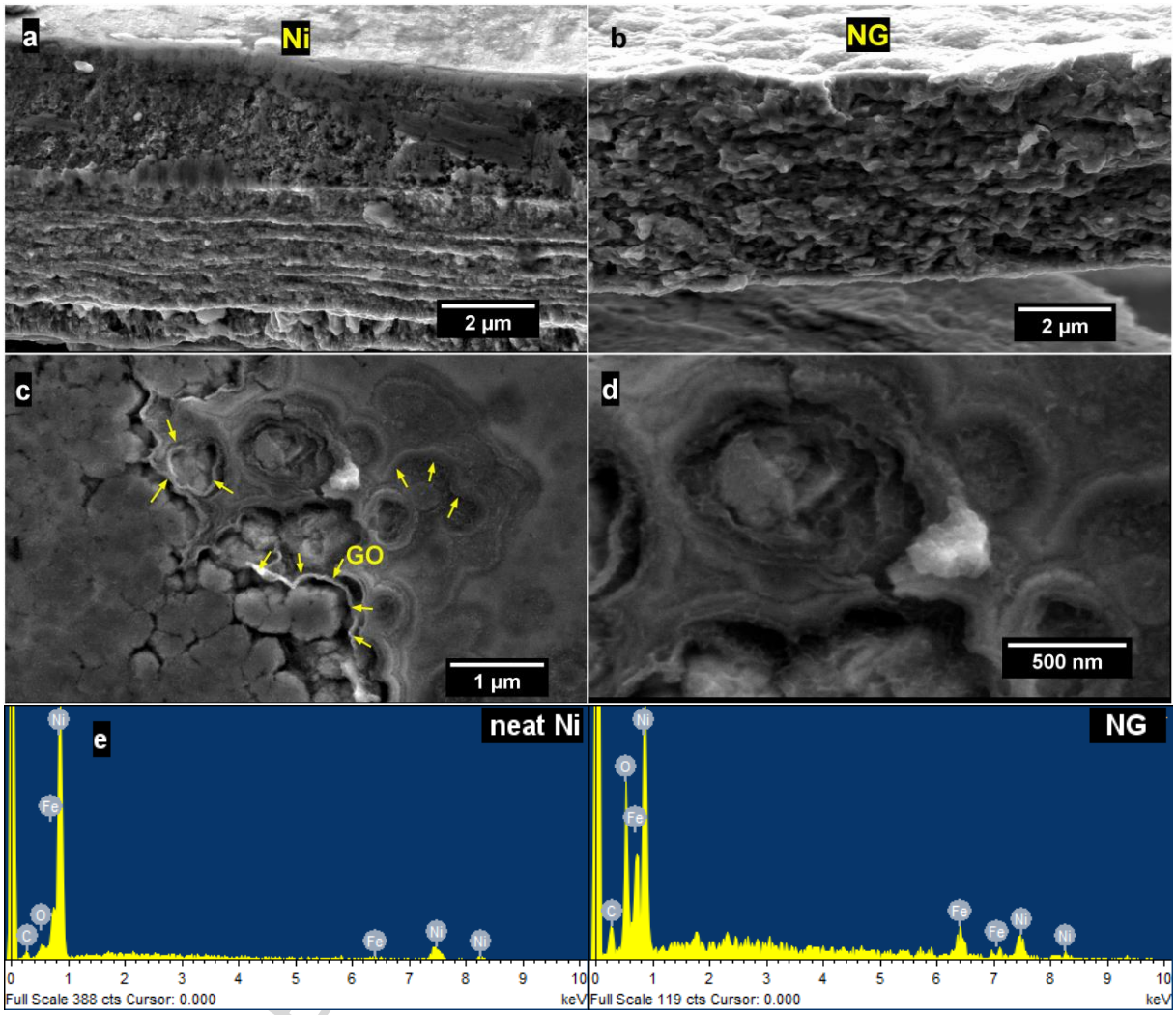

Figure 3

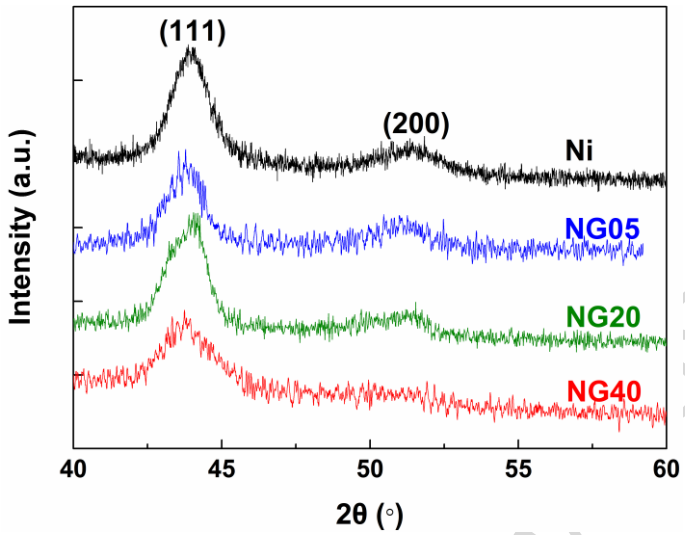

Figure 4

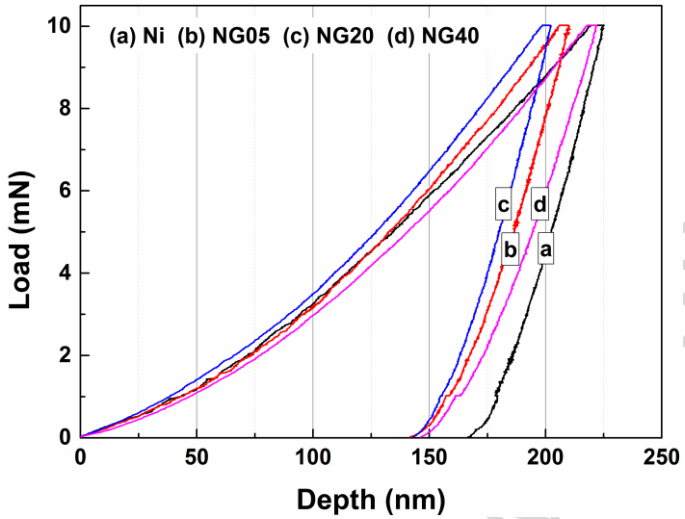

Figure 5

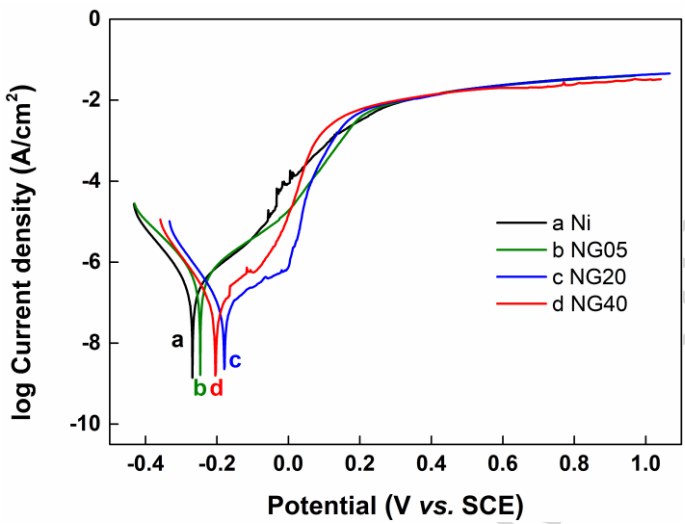

Figure 6

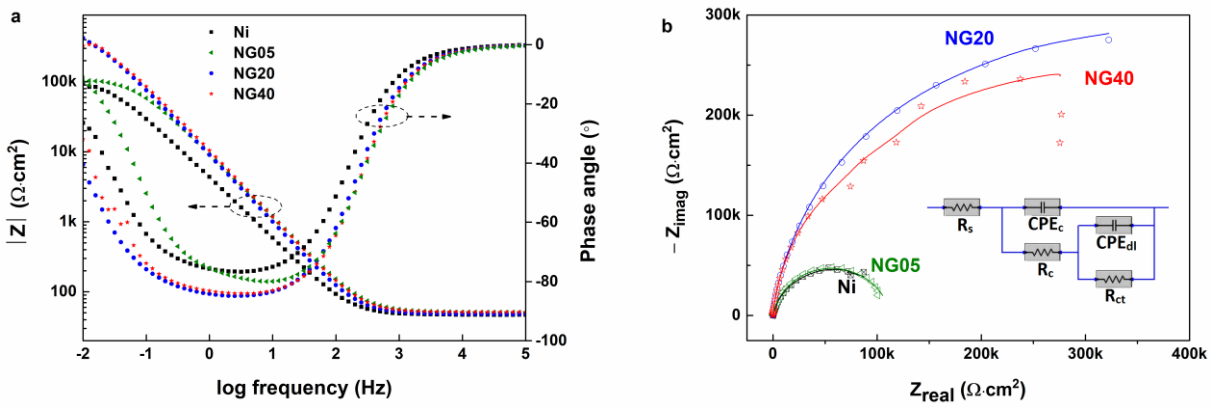

Figure 7

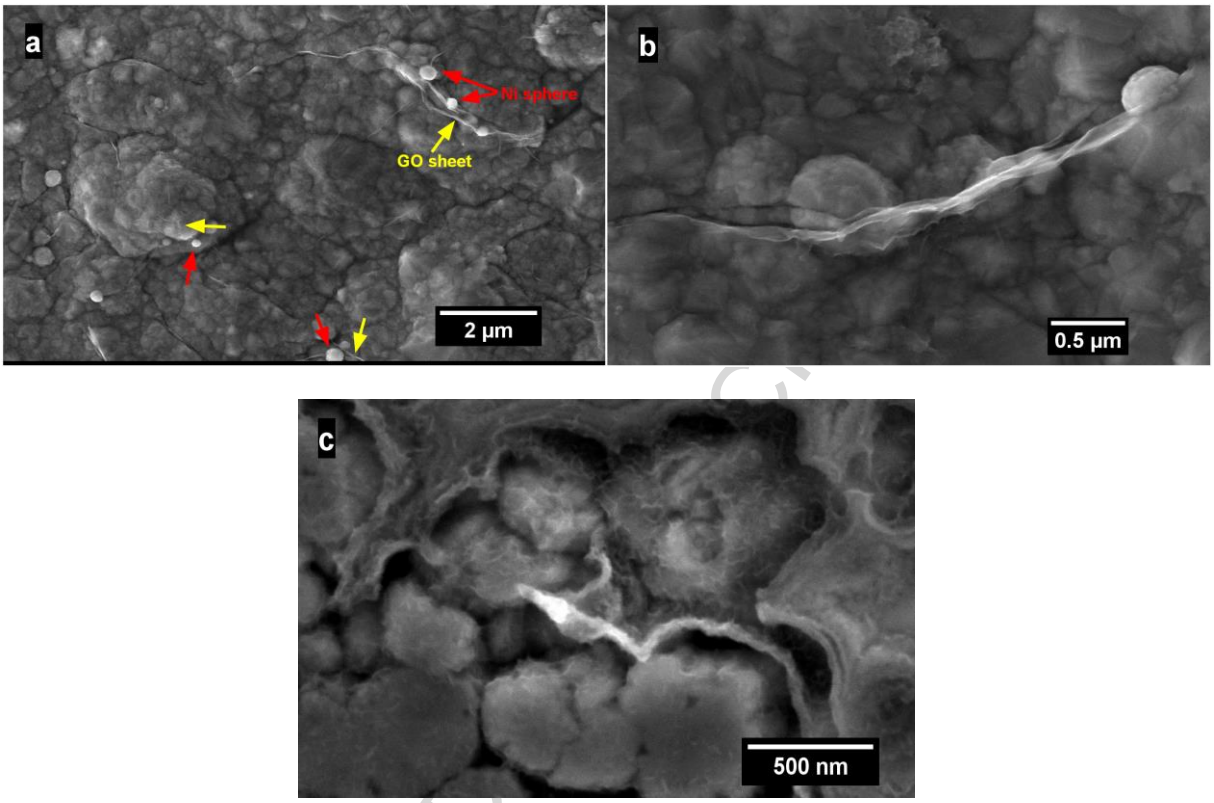

Figure 8

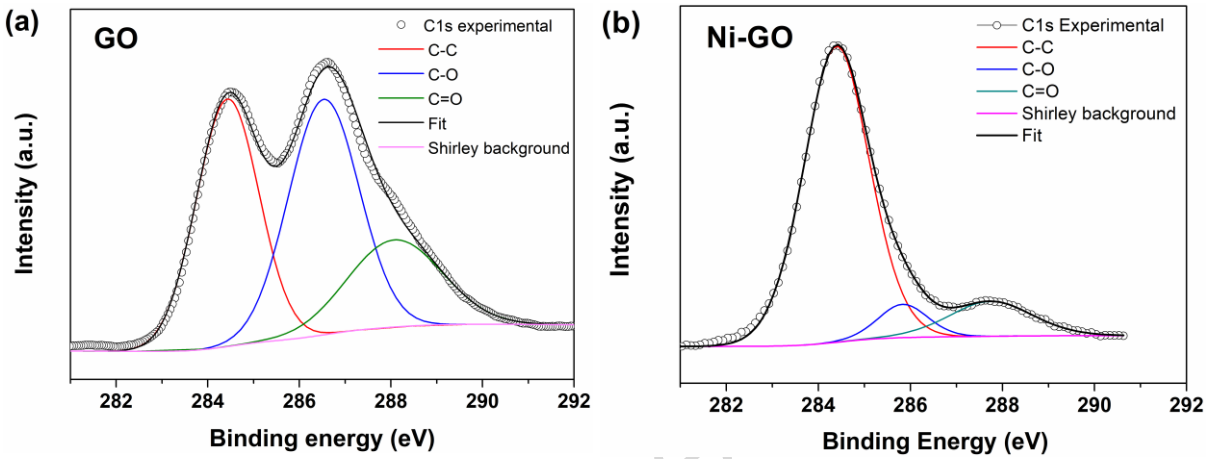

Figure 9

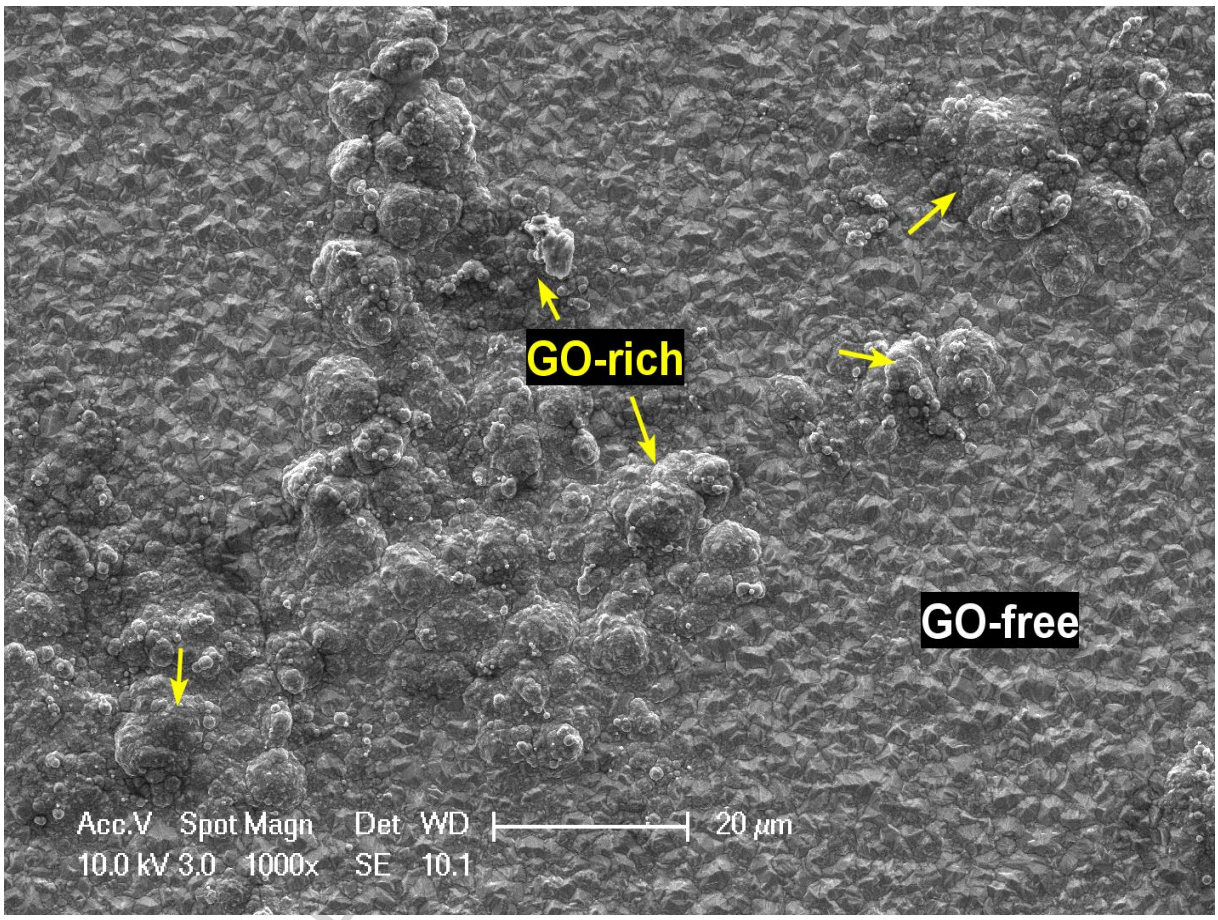

Figure 10

Table 1. The four plating solutions and the corresponding coatings in this work

GO content in solution (mg/ml)	0	0.5	2.0	4.0
Sample code	Ni	NG05	NG20	NG40

Table 2. Calculated crystallite size for neat Ni, NG05, NG20 and NG40 coatings

	(111) FWHM (degree)	grain size approx. (normalised)
Ni	1.1917	1
NG05	1.2327	0.97
NG20	1.3273	0.90
NG40	1.9879	0.60

Table 3. Nanoindentation results

Sample	Nano-hardness (GPa)	Reduced modulus (GPa)	Plasticity index
Ni	7.75±0.84	184.52±8.08	0.716±0.036
NG05	8.57±0.63	178.63±7.52	0.687±0.018
NG20	8.65±0.41	206.38±14.82	0.704±0.015
NG40	7.90±0.34	146.90±5.30	0.659±0.012

Table 4. Tafel fit parameters for the polarisation curves

Sample	OCP (mV)	E_{corr} (mV)	I_{corr} ($\times 10^{-9}$ A/cm^2)	Corrosion rate ($\times 10^{-3}$ mpy)
neat Ni	-232	-269	309	131.4
NG05	-230	-247	571	261.2
NG20	-133	-179	131	55.8
NG40	-158	-204	92.4	39.3

Table 5. Equivalent circuit fit parameters for the EIS samples

Sample	R_s ($\Omega \cdot cm^2$)	R_c ($k\Omega \cdot cm^2$)	CPE_c ($\mu S \cdot s^n \cdot cm^{-2}$)	n_1	R_{ct} ($k\Omega \cdot cm^2$)	CPE_{dl} ($\mu S \cdot s^n \cdot cm^{-2}$)	n_2
Ni	47.0	6.8	38.9	0.908	112	9.6	0.658
NG05	51.0	19.2	7.3	1	114	13.3	0.829
NG20	48.1	519	19.7	0.948	159	106	1
NG40	51.4	371	16.8	0.949	177	37.2	0.998

Highlights

- Electro-brush plating enabled homogeneous distribution of GO sheets in Ni matrix.
- Hardness and Young's modulus were improved and plasticity reduced.
- GO sheets enhanced the thermal stability of the composite coating.
- Corrosion resistance was improved due to GO and the mechanism discussed.